IEEE Access
Multidisciplinary | Rapid Review | Open Access Journal

Date of publication xxxx 00, 0000, date of current version xxxx 00, 0000.

Digital Object Identifier 10.1109/ACCESS.2024.Doi Number

High Stability Single-Port Dual Band Microwave Sensor Based on Interdigital Capacitor Structure with Asymmetry Branch Feedline

Syah Alam[1], (Member IEEE), Indra Surjati[1], (Member IEEE), Lydia Sari[1], (Member IEEE), R. Deiny Mardian[1], (Member IEEE), Teguh Firmansyah[2], (Member IEEE), Muhammad Iqbal[3], Slamet Widodo[4], Mudrik Alaydrus[5], (Senior Member IEEE), Zahriladha Zakria[6], (Senior Member IEEE)

[1]Department of Electrical Engineering, Universitas Trisakti, West Jakarta, Indonesia
[2] Department of Electrical Engineering, Universitas Sultan Ageng Tirtayasa, Kota Serang, Banten 42124, Indonesia
[3] Advanced Functional Materials Laboratory, Faculty of Industrial Technology, Institut Teknologi Bandung, Bandung 40132, Indonesia.
[4] Department of Mechanical and Biosystem Engineering, IPB University, Bogor 16680, Indonesia.
[5] Department of Electrical Engineering, Universitas Mercu Buana, West Jakarta, Indonesia
[6] Faculty of Electronic and Computer Technology and Engineering, Universiti Teknikal Malaysia Melaka (UTeM), Malaysia

Corresponding author: Syah Alam (e-mail: syah.alam@trisakti.ac.id) / Zahriladha Zakaria (zahriladha@utem.edu.my)

ABSTRACT This paper proposes a single-port interdigital capacitor (IDC) resonator based on asymmetric branch feed line with high stability performance for permittivity detection of solid materials with a permittivity range of 1 - 6.15. The microwave sensor is designed using a single-port resonator operating at two different resonant frequencies f_{r1} = 1.61 GHz and f_{r2} = 2.52 GHz. Dual band frequency was proposed using asymmetric branch feed line. In addition, to confine the electric field concentration of the resonator, an interdigital capacitor (IDC) structure is proposed as a solution. Furthermore, a copper shield was proposed as conducting material to evaluate performance stability of the sensor from disturbance effect with range of d = 1 cm – 2.5 cm. Based on the measurement results, the sensor has high stability both without and with disturbance with an a Frequency Detection Resolution (FDR) of 0.009 - 0.4 GHz/$\Delta\varepsilon_r$, a Normalized Sensitivity (NS) of 0.4% - 4.4%, and an average accuracy of 90% - 95% for both resonance frequencies, respectively. Therefore, this sensor can be recommended for several applications such as biomedical industry, pharmaceuticals and material quality control especially for outdoor measurements that are potentially affected by electromagnetic interference and disturbance.

INDEX TERMS Dual-band, high stability, interdigital capacitor, microwave sensor, single-port resonator

I. INTRODUCTION

Microwave sensors (MS) have seen significant advancement in the evaluation of both solids and liquids due to their advantages, such as high precision, a high Q-factor, cost-effectiveness, and compactness [1]–[3]. One of the measurable properties using MS is permittivity, which reflects a material's ability to sustain an electric field. The permittivity of the material under test (MUT) can be determined via perturbation theory, assuming the MUT behaves as a capacitive load [4]–[6]. Several microwave sensors based on resonators like the Split Ring Resonator (SRR) [7]–[10], Complementary Split Ring Resonator (CSRR)[11]–[13], Substrate Integrated Waveguide (SIW) [14],[15], Interdigital Capacitor (IDC) [16]–[20], AMC [21],[22] have been developed for solid and liquid material assessment.

Previous work presented a single-port MS based on slot loaded [23] and dual U-shaped [24] for solid material characterization. Furthermore, another work proposed a dual-function permittivity sensor with an antenna using a single-port resonator for solid material characterization using an aperture coupling structure [25]. In addition, previous work [26] proposed a single-port microwave sensor based on dual T-shaped for contact and long-distance detection. The advantage of a single-port resonator-based microwave sensor is that it can also function as an antenna for data transmission[27]. However, the performance of a

single-port resonator-based microwave sensor has a high potential to be inferred by electromagnetic waves and is also susceptible to disturbance. This is because the single-port resonator also transmits electromagnetic waves so that it is more susceptible to environmental disturbances, for example conducting materials. In addition, another limitation is that there is a higher likelihood of interference between the input and reflected signals. This can lead to difficulties and instability in the accuracy of representing measurement data. Therefore, a single-port resonator-based microwave sensor with high stability is needed to obtain accurate and reliable measurement results.

This work provides an excellent solution by proposing a high stability single-port MS based on Interdigital Capacitor (IDC) structure. The MS is designed to operate at two different frequencies f_{r1} = 1.61 GHz and f_{r2} = 2.52 GHz using an asymmetric branch feed line while the IDC structure is used to confine the concentration of the E-field in the sensing area so that the sensor is more focused on detecting samples. Furthermore, to observe the performance stability of the proposed sensor, a rectangular copper shield as conducting material is placed right above the sensor surface with a distance range of d = 1 cm - 2.5 cm to emulate as a disturbance. The performance of the sensor observed in this work is related to frequency shift, ΔF, Frequency Detection Resolution (FDR), Normalized Sensitivity (NS) and average accuracy. In addition, an interdigital capacitor structure also can minimize the H-field distribution so that the highest E-field concentration is focused on the sensing area of the proposed sensor. From the measurement results, the proposed sensor has high stability both without and with disturbance for a distance range of d = 1 - 2.5 cm. The sensor has stable performance with a frequency detection resolution of 0.009 - 0.4 GHz/Δε$_r$, a normalized sensitivity of 0.4% - 4.4%, and an average accuracy of 90% - 95% for both resonance frequencies, respectively.

II. WORKING PRINCIPLE OF PROPOSED SENSOR

This section explains the structure, equivalent circuit and sensing area location determination of the IDC resonator using asymmetric branch feedline.

A. DEVELOPMENT MODEL OF PROPOSED RESONATOR

Furthermore, to estimate the performance of the resonator having dual band characteristics, a development model of the proposed resonator was represented as shown in **Fig. 1**. The 1st model of the resonator is represented by a T-shaped resonator operating at a single band at a frequency of 2.26 GHz. Furthermore, the 2nd model is represented by a T-shaped connected with two open-ended inductive arms that function as branch lines that generate a single band resonant frequency of 1.16 GHz. The resonant frequency of the resonator moves to a lower frequency in line with the increase in the arm length of the resonator. In the 3rd model, the IDC structure is connected with two open-ended inductive arms of the resonator that produce dual-band characteristics with f_{r1} = 1.62 GHz and f_{r2} = 2.42 GHz.

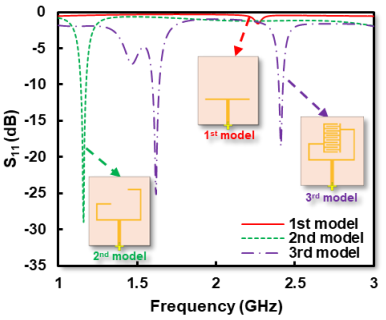

FIGURE 1. Development model of proposed resonator, (a) 1st model, (b) 2nd model, (c) 3rd model

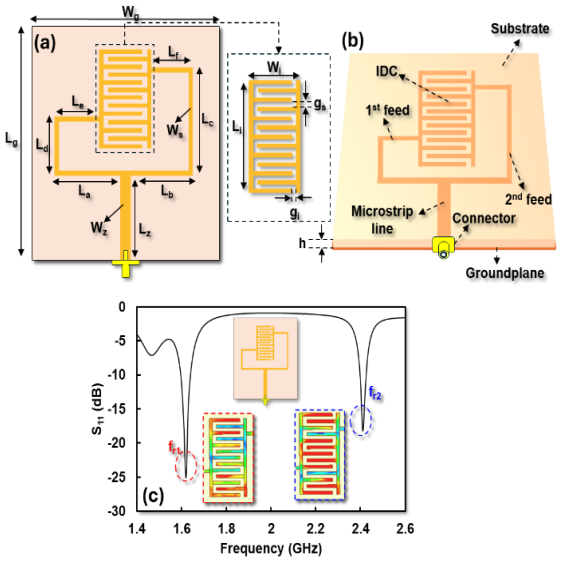

FIGURE 2. Model of the microwave sensor; (a) dimensions of the microwave sensor, (b) structure of the microwave sensor, (c) simulation of the reflection coefficient of the microwave sensor.

B. STRUCTURE OF PROPOSED IDC RESONATOR USING ASYMMETRY BRANCH FEED LINE

The proposed microwave sensor is designed using FR-4 substrate type with dielectric constant (ε$_r$) 4.3, loss tan (tan α) 0.0265 and thickness (h) 1.6 mm. The microwave sensor is designed using a single-port resonator operating at two different resonant frequencies f_{r1} = 1.62 GHz and f_{r2} = 2.42 GHz. To produce dual frequencies, the resonator is connected with RP-SMA connector with impedance of 50 Ω using dual-feed approach.

In addition, to increase the electric field concentration of the resonator, interdigital capacitor (IDC) structure is proposed as a solution. **Fig. 2 (a)** shows the dimensions of the proposed sensor. Furthermore, **Fig. 2 (b)** shows the structure of the proposed sensor where the sensor is designed using a PCB with two copper layers while the upper layer of the PCB is used to place the sensor made of copper and the

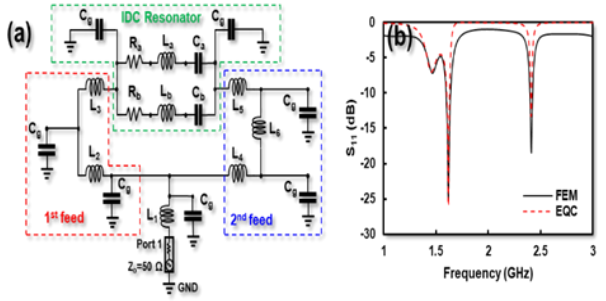

FIGURE 3. Modeling of the proposed sensor; (a) Equivalent circuit of the proposed sensor, (b) comparison of simulation results from FEM and EQC.

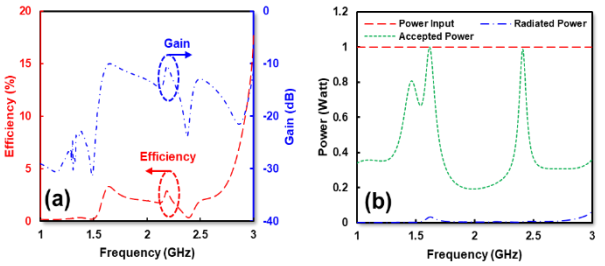

FIGURE 4. Simulation result of single port resonator, (a) efficiency and gain of proposed resonator, (b) comparison between input, accepted dan transmitted power of proposed resonator

lower layer is used as a ground plane. The simulation results of the proposed sensor are shown in **Fig. 2 (c)** where the sensor operates at two different resonant frequencies, namely f_{r1} = 1.62 GHz and f_{r2} = 2.42 GHz.

The dimensions of the proposed sensor are represented by W_g = 50 mm, L_g = 50 mm, W_s = 3.1 mm, L_z = 15 mm, L_a = 17.3 mm, L_b = 15.9 mm, W_s = 1 mm, L_c = 26.7 mm, L_d = 13.7 mm, L_e = 11.8 mm and L_f = 11.8 mm. Furthermore, the dimensions of the IDC structure are represented by W_i = 11.7 mm and L_i = 25 mm while the gaps in each IDC are represented by G_i = G_s = 1 mm. It should be noted that the width and length of the gap greatly affect the electric field concentration and the resonant frequency of the proposed sensor.

The performance in terms of gain and efficiency of the single port resonator are shown in **Fig. 4(a)** and **Fig. 4(b)**. Furthemore, **Fig. 4 (a)** shows that the proposed resonator has low efficiency at f_{r1} = 1.61 GHz and f_{r2} = 2.42 GHz of 3.04% and 0.68%, respectively. In addition, the gain of proposed resonator is also very low where for f_{r1} = 1.62 GHz and f_{r2} = 2.42 GHz it is -10.37 dB and -16.63 dB, respectively. Furthermore, the ratio between the input power, received power and transmitted power of the proposed resonator is also very low as shown in **Fig. 4 (b)**. From the simulation results, the default input power is 1 watt while the transmitted power for f_{r1} = 1.62 GHz and f_{r2} = 2.42 GHz is 0.98 watt and 0.97 watt. However, the transmitted power is very low where for f_{r1} = 1.62 GHz and f_{r2} = 2.42 GHz is 0.03

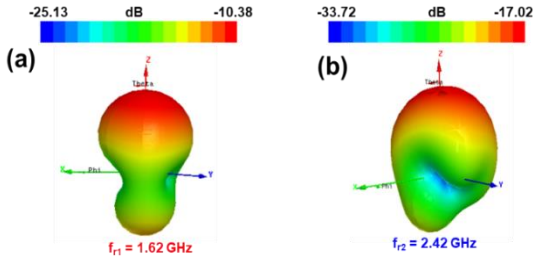

FIGURE 5. Simulation result of radiation pattern, (a) radiation pattern at f_{r1} = 1.62 GHz, (b) radiation pattern at f_{r2} = 2.42 GHz

watt and 0.006 watt, respectively. Furthermore, the radiation pattern of the proposed resonator is shown in **Fig. 5 (a)** and **Fig. 5 (b)** where f_{r1} = 1.62 GHz and f_{r2} = 2.42 GHz have a maximum gain of -10.38 dB and -17.02 dB. This finding indicates that the proposed resonator has low performance to function as an antenna due to low efficiency and gain. Thus, this structure is more suitable for microwave sensors.

C. EQUIVALENT CIRCUIT MODEL OF PROPOSED RESONATOR

Next, the proposed sensor can be modeled using an equivalent circuit (EQC) based on resistor (R), capacitor (C) and inductor (L) [28] as shown in **Fig. 3 (a)**. The equivalent circuit of the proposed sensor is calculated and simulated using AWR 2009 and compared with Finite Element Modeling (FEM) as shown in **Fig. 3 (b)**. Based on the equivalent circuit shown in **Fig. 3 (a)**, the feedline of the resonator is represented by L_1 = 14 nH which is connected to port 1 with an impedance of Z_0 = 50Ω. In this work, the asymmetric branch feedline is represented by L_2 = 15.3 nH and L_3 = 0.71 nH as the 1st arm while the 2nd arm is represented by L_4 = 0.000242 nH, L_5 = 20.89 nH and L_6 = 9.18 nH. In addition, the IDC resonator is represented by two resonators with series configuration connected in parallel where R_a = 0.027 kΩ, L_a = 41.97 nH, C_a = 805 pF while for R_b = 2.46 kΩ, L_b = 0.262 nH and C_b = 6.28 pF. To prevent short circuits, C_g = 1 pF is proposed as grounding. Overall, the resonant frequency of the resonator can be determined using the following equation [27]:

$$f_r = \frac{1}{2\pi\sqrt{LC}} \quad (1)$$

Fig. 3 (b) shows that the simulation results of EQC and FEM have identical characteristics where the resonator operates in dual band with f_{r1} = 1.62 GHz and f_{r2} = 2.42 GHz. This finding indicates that the proposed equivalent circuit model has represented the working principle of the proposed resonator.

D. SENSING AREA DETERMINATION

In this work, the sensor is designed to detect the permittivity of the sample by observing the interaction between the electric field and the permittivity of the sample used. The resonator surface that has a high electric field (E-field) can

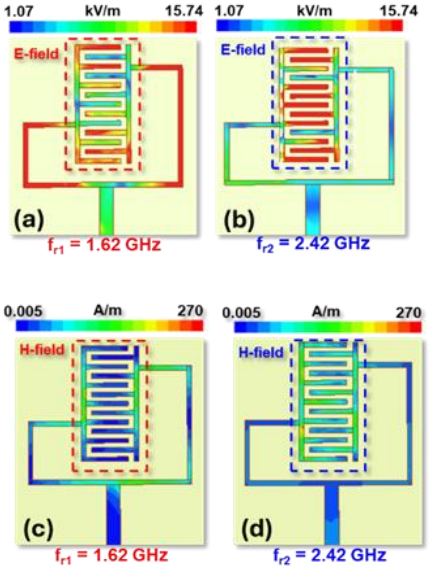

FIGURE 6. E-field and H-field simulations; (a) E-field at f_{r1} = 1.62 GHz, (b) E-field at f_{r2} = 2.41 GHz, (c) H-field at f_{r1} = 1.62 GHz, (d) H-field at f_{r2} = 2.42 GHz

be recommended as the sensing area used to place the sample. The sample used is a dielectric sample that does not contain metal. Furthermore, the electric field and magnetic field concentrations of the IDC-based resonator are shown in **Fig.6 (a)**, **Fig.6 (b)**, **Fig.6 (c)** and **Fig.6 (d)**.

Furthermore, **Fig. 6 (a)** and **Fig. 6 (b)** show that the highest electric field concentration of the proposed resonator at f_{r1}=1.62 GHz and f_{r2}= 2.42 GHz is on the IDC surface of the proposed sensor with a range of 1.07 – 15.74 kV/m. In contrast, the magnetic field concentration of the proposed resonator at f_{r1}=1.62 GHz and f_{r2}= 2.42 GHz are very low and is in the range of 0.005 – 270 A/m as shown in **Fig. 6 (c)** and **Fig. 6 (d)**. These findings indicate that the IDC surface has a high electric field and a low magnetic field so that it becomes a potential location as a sensing area that can be recommended to place samples to be detected. It also shows that the application of the IDC structure has successfully confined the electric field and reduced the magnetic field in the proposed sensor.

Moreover, **Fig. 7 (a)** shows the scenario of dielectric sample placement on the proposed sensor. In this work, the dielectric sample is placed in the sensing area determined based on the highest E-field concentration with dimensions of 10.7 mm x 23 mm x 1 mm. The samples used consist of four types of dielectrics with different permittivity where RO5880 is 2.2, RO4003C is 3.65, FR4 is 4.3 and RO3006 is 6.15. The proposed sensor is connected to a Vector Network Analyzer (VNA) and a PC using a coaxial cable and a USB cable with a frequency range of 1 - 3 GHz and a span of 0.001 GHz. The frequency response of f_{r1} and f_{r2} based on the permittivity change of the dielectric sample is shown in **Fig. 7 (b)**. Overall, the resonant frequencies of f_{r1} = 1.62 GHz and

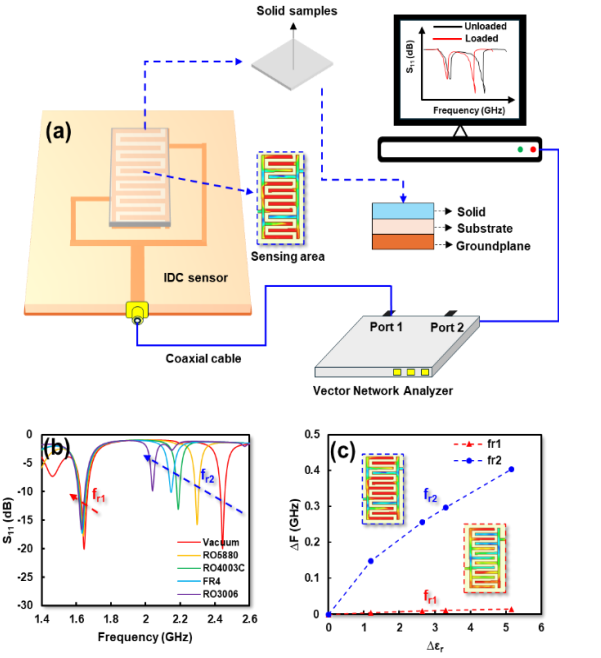

FIGURE 7. (a) Scenario of sample placement of proposed sensor, (b) simulation result of resonance frequency f_{r1} and f_{r2} with permittivity changes, (c) ΔF of proposed sensor for f_{r1} and f_{r2}

f_{r2} = 2.42 GHz shift to low frequencies in line with the increase of the permittivity of the sample. Based on the simulation results, f_{r1} shifts from 1.64 GHz to 1.63 GHz while for f_{r2} it shifts from 2.42 GHz to 2.02 GHz for the permittivity range of 1 - 6.15. Furthermore, the ΔF of f_{r1} and f_{r2} are shown in **Fig. 7(c)** where for f_{r1} and f_{r2} are 0.01 GHz and 0.4 GHz, respectively.

These findings indicate that the proposed sensor can sense the permittivity change of the dielectric sample based on the frequency change. The resonant frequency of the resonator moves toward the low frequency in line with the increase in the permittivity of the dielectric sample. In addition, f_{r2} is more sensitive than f_{r1} because it has a higher frequency [2] and has a higher electric field concentration compared to f_{r1} as shown in **Fig. 7 (c)**.

III. MEASUREMENT RESULT AND VERIFICATION

This section will discuss the measurement and validation of the proposed sensor, the performance and response of the proposed sensor based on the analysis of the disturbance effects. In this work, the proposed sensor is given a rectangular copper shield disturbance placed on the surface of the sensor.

A. MEASUREMENT OF PROPOSED SENSOR

The next stage is to validate the performance of the proposed sensor to characterize solid materials. In this work, the samples used are solid materials whose permittivity has been known based on the datasheet with a range of 1 - 6.15. Solid materials used as samples include RO5880 with a permittivity of 2.2, RO4003C with a permittivity of 3.65, FR4 with a permittivity of 4.3 and RO3006 with a

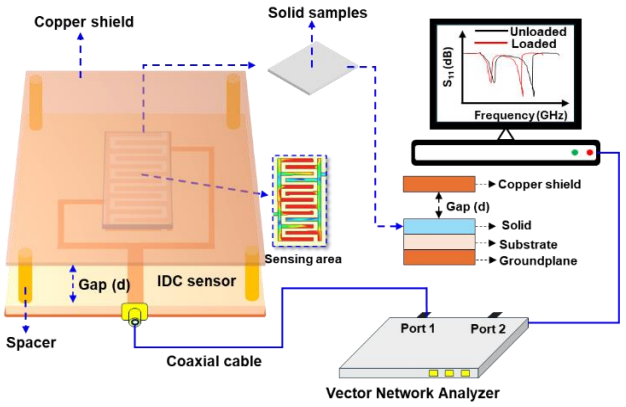

FIGURE 8. Scenario of placing a solid sample on the proposed sensor with copper shield.

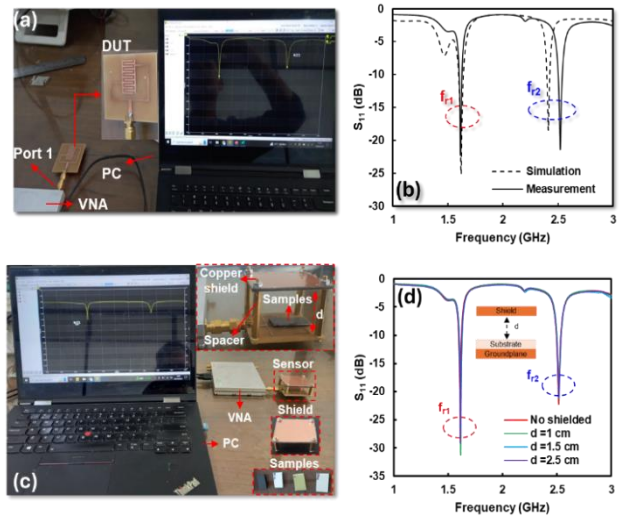

FIGURE 9. Measurement of the proposed sensor; (a) measurement setup, (b) comparison of simulation and measurement, (c) measurement setup of proposed sensor with copper shield, (d) measurement result from proposed sensor with and without shield

permittivity of 6.15. The dimensions of the samples used are adjusted to the location of the sens ing area of the proposed sensor, which is 12.7 mm x 25 mm with a sample thickness of 1.6 mm. The measurement scenario and placement of solid samples on the proposed sensor are shown in **Fig. 8**. In this work, the solid sample with dimensions of 10.7 mm x 23 mm x 1.6 mm is placed on the sensing area surface protected by a rectangular copper shield with dimensions of 50 x 50 mm x 1.58 mm. The copper shield is placed using a brass spacer placed at a certain distance represented by *d*. It should be noted that the copper shield is proposed as disturbance and also focuses on the electric field so that it is fully concentrated on the sample. The measurement process of the sensor is carried out in the laboratory using a VNA measuring instrument connected to the sensor using a coaxial cable via port 1 while the reading of the measurement results

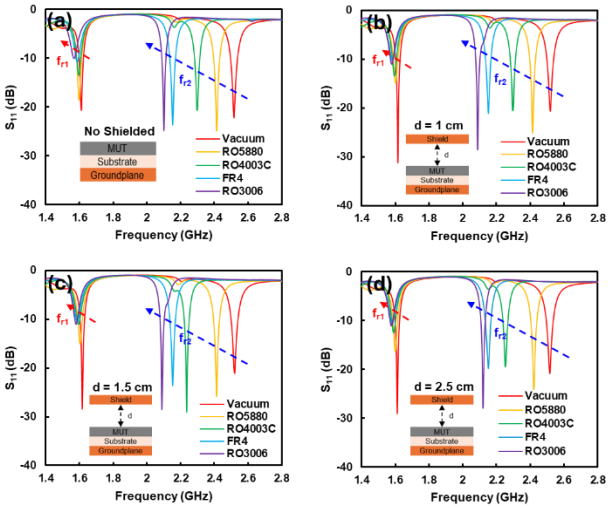

FIGURE 10. Shift of resonance frequency of proposed sensor; (a) without shielded, (b) with cooper shielded of *d* = 1 cm, (c) with cooper shielded of *d* = 1.5 cm, (d) with cooper shielded of *d* = 2.5 cm

is carried out using a PC connected to the VNA via a USB cable. The measurement process is carried out in a closed room with an ambient temperature of 25˚C as shown in **Fig. 9 (a)**. Next, a comparison of the simulation and measurement results of the proposed sensor is shown in **Fig. 9 (b)**. From the measurement results shown in **Fig. 9 (b)**, f_{r1} shifts from 1.62 GHz to 1.61 GHz while f_{r2} shifts from 2.42 GHz to 2.52 GHz. These findings indicate that the proposed sensor has identical performance between simulation and measurement with error rates of 0.6% and 4.1% for f_{r1} and f_{r2}, respectively.

Moreover, the measurement setup of the sensor with a copper shield with a distance of d = 1 – 2.5 cm is shown in **Fig. 9 (c)**. Based on measurement results, the resonant frequencies of f_{r1} and f_{r2} are fixed and not affected by the copper shield placed right above the proposed sensor as shown in **Fig. 9 (d)**.

B. PERFORMANCE OF PROPOSED SENSOR WITH ANALYSIS DISTURBANCE EFFECT

In this work, disturbance in the form of rectangular copper shield is placed above the sensor with a distance range of d = 1 - 2.5 cm. The performance of the sensor is observed based on the shift in resonance frequency based on the permittivity of the dielectric sample placed in the sensing area. Furthermore, the four solid material samples are placed right above the sensing area surface of the sensing area where the sensor condition without sample (vacuum) with ε_r of 1 is used as a reference. In addition, the effects of disturbance are also observed separately when the sensor is without copper shield and using copper shield with a distance of d = 1 cm - 2.5 cm as shown in **Fig. 10 (a)**, **Fig. 10 (b)**, **Fig. 10 (c)** and **Fig. 10 (d)**. Furthermore, the frequency shift of the sensor (ΔF), normalized sensitivity and frequency detection resolution (FDR) which is determined based on the following equation[29] [30]:

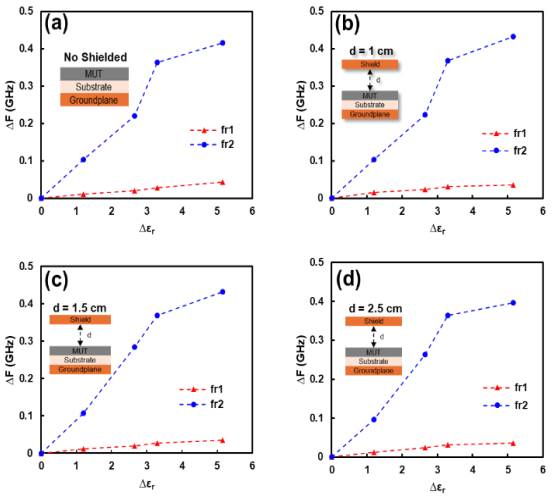

FIGURE 11. ΔF of proposed sensor; (a) without shielded, (b) with cooper shielded of *d* = 1 cm, (c) with cooper shielded of *d* = 1.5 cm, (d) with cooper shielded of *d* = 2.5 cm

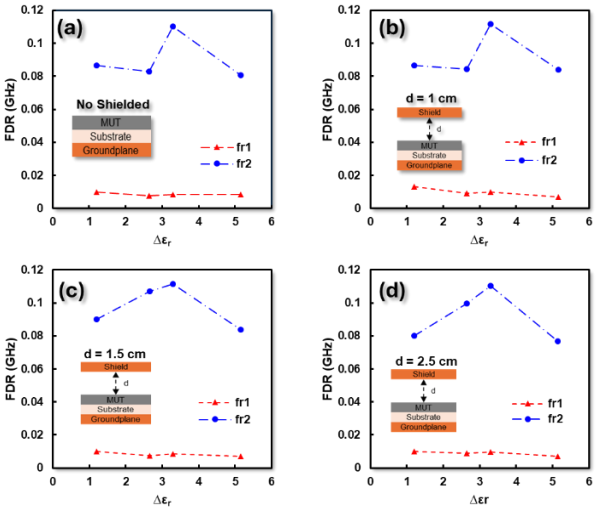

FIGURE 12. Frequency detection resolution of proposed sensor; (a) without shielded, (b) with cooper shielded of *d* = 1 cm, (c) with cooper shielded of *d* = 1.5 cm, (d) with cooper shielded of *d* = 2.5 cm

$$\Delta f = (f_{unloaded} - f_{loaded})\ GHz \quad (2)$$

$$NS = \frac{1}{\Delta\varepsilon_r}\left(\frac{f_{unloaded} - f_{loaded}}{f_{unloaded}}\right)\% \quad (3)$$

$$FDR = \frac{\Delta F}{\Delta\varepsilon_r}\ GHz \quad (4)$$

where ΔF represents the frequency shift range, $f_{unloaded}$ is the resonance frequency when the sensor is in a vacuum condition while f_{loaded} is the frequency of the sensor when the sample is loaded, NS is the normalized sensitivity and $\Delta\varepsilon_r$ is the difference between the permittivity of the reference sample and the permittivity of the sample loaded to the sensor.

Furthermore, the correlation between the resonant frequency and permittivity changes of the four dielectric samples for shielded condition is shown in **Fig.10 (a)** where f_{r1} shifts from 1.62 GHz to 1.56 GHz while for f_{r2} shifts from 2.52 GHz to 2.1 GHz for the permittivity range of 1 - 6.15. Furthermore, the performance of the sensor with copper shielding for *d* = 1 cm and *d* = 1.5 cm is shown in **Fig. 10 (b)** and **Fig. 10 (c)** where f_{r1} shifts from 1.61 GHz to 1.58 GHz while for f_{r2} from 2.52 GHz to 2.02 GHz, respectively. In line with the previous, f_{r1} shifts from 1.61 GHz to 1.58 GHz and f_{r2} from 2.52 to 2.12 GHz for *d* = 2.5 cm as shown in **Fig. 10 (d)**. The resonant frequency shift of the sensor is represented as ΔF which can be determined using **Eq. (2)**. Furthermore, ΔF of the proposed sensor is shown in **Fig. 11(a)**, **Fig. 11(b)**, **Fig. 11(c)** and **Fig. 11(d)**.

From the measurement results, the maximum ΔF of the proposed sensor has a stable performance where for f_{r1} is 0.03 GHz and f_{r2} is 0.4 GHz for conditions with or without copper shielding. In addition, the same findings for the Frequency Detection Resolution (FDR) of the proposed sensor which can be determined using **Eq. (4)** where for the maximum FDR for f_{r1} is 0.009 GHz / $\Delta\varepsilon_r$ while for f_{r2} is 0.11 GHz / $\Delta\varepsilon_r$ for both conditions with or without shielding as shown in **Fig. 12(a)**, **Fig. 12(b)**, **Fig. 12(c)** and **Fig. 12(d)**.

These findings indicate that the performance of the proposed sensor is not significantly affected by the addition of disturbance in the form of a copper shield. ΔF and FDR of the proposed sensor are relatively stable to detect the permittivity of dielectric samples with a permittivity range of 1 - 6.15.

The normalized sensitivity (NS) of the proposed sensor can be determined based on **Eq. (3)**. Furthermore, the NS of the proposed sensor for conditions with or without copper shield are shown in **Fig. 13 (a)**, **Fig. 13 (b)**, **Fig. 13 (c)** and **Fig. 13 (d)**. Based on the measurement results, the NS for the sensor with the condition without copper shield is in the range of 0.53% - 0.62% for f_{r1} while for f_{r2} it is in the range of 3.21% - 4.38% as shown in **Fig. 13(a)**. Furthermore, the NS for the sensor condition with copper shield for *d* = 1 cm is in the range of 0.43% - 0.83 for f_{r1} and f_{r2} in the range of 3.33 - 4.43% as shown in **Fig. 13 (b)**. In addition, the NS for the sensor with copper shield condition for *d* = 1.5 cm is in the range of 0.43% - 0.62% for f_{r1} while for f_{r2} is in the range of 3.33% - 4.43% as shown in **Fig. 13 (c)**. Finally, the NS for the sensor with copper shield for d = 2.5 cm is presented by **Fig. 13 (d)** where f_{r1} is in the range of 0.43% - 0.62% while for f_{r2} is in the range of 3.06% - 4.38%.

This finding indicates that the NS of the sensor with copper and without shield is stable because the electric field is more concentrated in the sensing area of the proposed sensor. This finding is also in line with the simulation where the E-field concentration of the IDC-based sensor is more dominant compared to the H-field so that the electric field from the sensor is focused in the sensing area of the sensor. In addition, the NS of the sensor without and with copper shield for the range *d* = 1 cm - 2.5 cm has a stable performance in

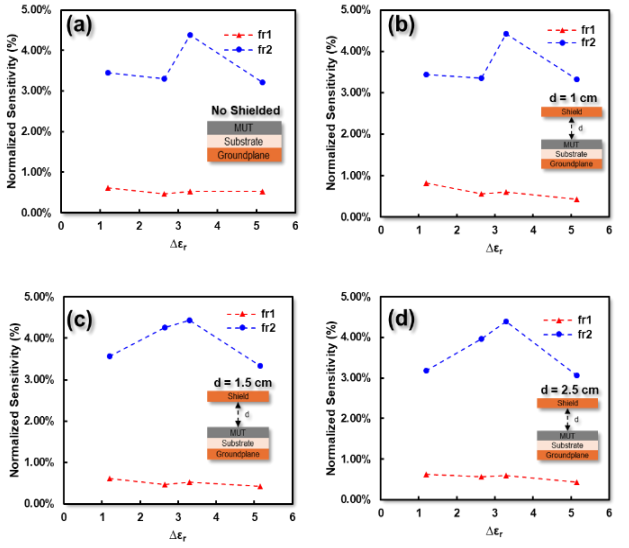

FIGURE 13. Normalized sensitivity of proposed sensor; (a) without shielded, (b) with cooper shielded of *d* = 1 cm, (c) with cooper shielded of *d* = 1.5 cm, (d) with cooper shielded of *d* = 2.5 cm

the range of 0.4% - 0.8 % and 3% - 4% for f_{r1} and f_{r2}, respectively .

This finding also shows that the addition of copper shield with a range of d = 1 cm - 2.5 cm as a disturbance has no significant effect on the performance of the proposed sensor and can be used to confined the electric field of the proposed sensor in the specific sensing area.

C. ACCURACY OF PROPOSED SENSOR

Furthermore, the correlation between resonance frequency and permittivity can be derived into a third-order polynomial equation that can be used to determine the permittivity of solid materials [31]–[33] as shown in **Fig.14 (a)**, **Fig. 14(b)**, **Fig. 14(c)**, **Fig. 14(d)**, **Fig. 14(e)**, **Fig. 14(f)**, **Fig. 14(g) and Fig. 14(h)**. Based on the correlation between the resonant frequency and permittivity from the measurement result, the permittivity of the dielectric sample for the condition without copper shielding can be determined based on the third-order polynomial equation as follows:

$$\varepsilon_{r1} = a_1 {f_{r1}}^3 + a_2 {f_{r1}}^2 - a_3 f_{r1} + a_4 \quad (4)$$

$$\varepsilon_{r2} = b_1 {f_{r2}}^3 + b_2 {f_{r2}}^2 - b_3 f_{r2} + b_4 \quad (5)$$

where ε_{r1} is the permittivity of the sample based on f_{r1} and ε_{r2} is the permittivity based on f_{r2}. Furthermore, based on the third order polynomial equation, the values of a_1 = -78.685, a_2 = 174.14, a_3 =75667, a_4 = 0, b_1 = -156.76, b_2 =1091.2, b_3 =2537 and b_4 =1973.3 are obtained for conditions without copper shield as shown in **Fig. 14 (a)** and **Fig. 14 (b)**. Next, for d = 1 cm the values are obtained from a_1 = -143572, a_2 = 691050, a_3 =1E+06, a_4 = 593083, b_1 = -133.95, b_2 =930.72, b_3 =2161.1 and b_4 =1680 while for d = 1.5 cm the values are obtained from a_1 = -54026, a_2 = 260387, a_3 =418443, a_4 = 224209, b_1 = -125.03, b_2 =876.5 , b_3 = 2053.8 and b_4 =1611.1 as shown in **Fig. 14 (c), Fig. 14 (d)**, **Fig. 14 (e)** , **Fig. 14 (f)**. Finally, for the condition d = 2.5 cm the values are obtained from a_1 = -19381, a_2 = 928985, a_3 = -1E+06, a_4 = 790597, b_1 = -188.7, b_2 =1323.7 , b_3 = -3100 and b_4 =2426.3 as shown in **Fig. 14 (g)** and **Fig. 14 (h)**. Overall, the permittivity based on calculations for f_{r1} and f_{r2} is shown in **Table I** and **Table II**.

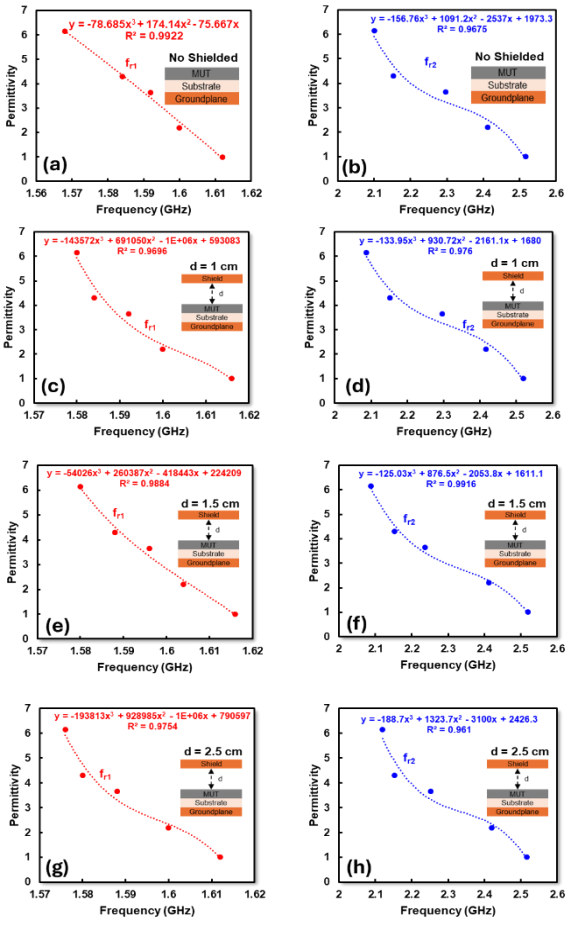

FIGURE 14. Polynomial equation based on resonant frequency and permittivity; (a) without shielded for f_{r1}, (b) without shielded for f_{r2}, (c) with cooper shielded of d = 1 cm for f_{r1}, (d) with cooper shielded of d = 1 cm for f_{r2}, (e) with cooper shielded of d = 1.5 cm for f_{r1}, (f) with cooper shielded of d = 1.5 cm for f_{r2}, (g) with cooper shielded of d = 2.5 cm for f_{r1}, (h) with cooper shielded of d = 2.5 cm for f_{r2}

TABLE I
ACCURACY OF PROPOSED SENSOR FOR 1ST RESONANT FREQUENCY

	No shielded		Shielded cooper					
			d = 1 cm		*d* = 1.5 cm		*d* = 2.5 cm	
ε_r reference	ε_r calc.	Acc. (%)	ε_r calc.	Acc. (%)	ε_r calc.	Acc. (%)	ε_r calc.	Acc. (%)
1	0.94	93.54	0.98	98.25	0.97	97.36	0.97	97.20
2.2	2.44	89.21	2.39	91.51	2.37	92.13	2.33	93.92
3.65	3.41	93.32	3.23	88.61	3.34	91.46	3.32	90.84
4.3	4.35	98.86	4.77	89.14	4.52	94.82	4.75	89.50
6.15	6.16	99.86	5.93	96.39	6.09	99.06	5.93	96.37

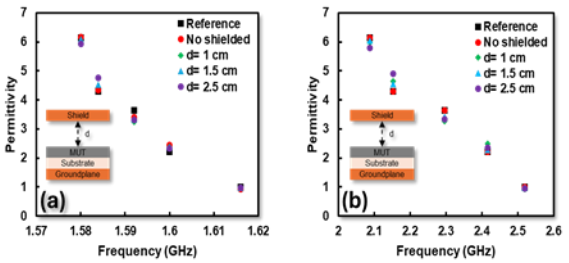

FIGURE 15. Accuracy of proposed sensor; (a) without shielded, (b) with cooper shielded of d = 1 cm, (c) with cooper shielded of d = 1.5 cm, (d) with cooper shielded of d = 2.5 cm

TABLE II
ACCURACY OF PROPOSED SENSOR FOR 2ND RESONANT FREQUENCY

ε_r reference	No shielded		Shielded cooper					
			d = 1 cm		d = 1.5 cm		d = 2.5 cm	
	ε_r calc.	Acc. (%)	ε_r calc.	Acc. (%)	ε_r calc.	Acc. (%)	ε_r calc.	Acc. (%)
1	0.91	91.39	0.92	91.73	0.97	97.26	0.95	94.94
2.2	2.51	86.00	2.48	87.11	2.28	96.21	2.34	93.52
3.65	3.23	88.58	3.27	89.57	3.44	94.11	3.33	91.35
4.3	4.72	90.12	4.64	92.04	4.56	93.96	4.89	86.24
6.15	5.92	96.31	5.99	97.36	6.05	98.36	5.78	94.01

Based on **Table I** and **Table II**, the proposed sensor has good average accuracy where for the condition without copper shield it is at 94.96% and 90.48% for f_{r1} and f_{r2}, respectively. Furthermore, the average accuracy for f_{r1} and f_{r2} for the sensor with copper shield is 92.78% and 91.72% for d = 1 cm and for d = 1.5 cm the average accuracy is 94.97% and 95.98% while for d = 2.5 cm, the average accuracy is at 93.57% and 92.01%, respectively.

This finding shows that the best average accuracy is obtained when d = 1.5 cm. In addition, the sensor has a consistent average accuracy for conditions with and without shield. In addition, the sensor has a consistent average accuracy for conditions with and without shield compared with reference permittivity as shown in **Fig. 15 (a)** and **Fig. 15 (b)**. This finding also shows that the proposed sensor has high performance and is not significantly affected by disturbances placed directly above the sensor with range of d = 1 cm – 2.5 cm.

IV. VALIDATION WITH PREVIOUS WORKS

A thorough evaluation comparing the proposed sensor's performance with previous studies is conducted, as detailed in **Table III**. A fair comparison with previous work is proposed by observing the performance of the sensor in terms of the method, permittivity range, resonance frequency (f_r), Frequency Detection Resolution (FDR), Normalized Sensitivity (NS) and accuracy. In addition, other performances that are compared are dual band characteristics, e-field localization, disturbance effect analysis and also high stability of the proposed sensor.

Previous work proposed a microwave sensor using a dual-port resonator for permittivity detection of solid materials based on SRR [8],[10],[32], IDC structure [19],[20] and CSRR[13]. The sensor has good performance with a maximum accuracy of 96% - 98% and a normalized sensitivity of 1.34% - 5.38%. However, the proposed sensor only supports transmission mode-based measurements and requires a two-port network analyzer for characterization, which can increase the complexity and cost of the measurement setup.

Previous studies introduced a single-port resonator incorporating a slot for permittivity detection of dielectric samples, achieving an accuracy of 98.80% and a normalized sensitivity of 5.24% [23]. However, the sensor's electric field remains inadequately localized and focused on the sensing area, potentially leading to measurement inaccuracies in the presence of interference or disturbances. In addition, the proposed sensor only operates at a single resonant frequency. Moreover, a single-port microwave sensor with dual band performance utilizing U-shaped [24] and T-shaped resonators [26] was proposed in another study, featuring independent characteristics for simultaneous detection of solid material permittivity and long-distance sensing. The electric field of the resonator was localized on its arm, designated as the sensing area. However, the study did not include an analysis of disturbance effects, leaving the stability of the proposed sensor under disturbed conditions unverified.

Previous work introduced a single-port microwave sensor employing aperture coupling [25] and an artificial magnetic conductor [21]. The electric field was localized on a separate substrate, designated as the sensor's sensing area. However, the proposed structure features a multilayer design, making it more complex to implement. Furthermore, the study did not include an analysis of disturbance effects, leaving the sensor's stability under such conditions unverified. This work provides an excellent solution to produce a microwave sensor using a single-port resonator that has high stability against disturbances. In this work, an interdigital capacitor structure is introduced to confine the E-field of the sensor to focus it on the sensing area of the sensor. In addition, the interdigital capacitor structure also reduces the H-field so that the E-field becomes more dominant. The stability of the sensor is evaluated and confirmed by placing a disturbance in the form of a rectangular copper shield placed directly above the sensor. The performance and stability of the sensor are observed in conditions without and with copper shielding for a distance range of d = 1 cm - 2.5 cm. From the measurement results, the sensor has high stability both without and with disturbance with a Frequency Detection Resolution (FDR) of 0.009 - 0.4 GHz/$\Delta\varepsilon_r$, a Normalized Sensitivity (NS) of 0.4% - 4.4%, and an average accuracy of 90% - 95% for both resonance frequencies, respectively.

TABLE III
COMPARISON WITH PREVIOUS WORKS

Ref.	Method	Freq (GHz)	Range of ε_r	Performance			Num. of port	Dual-band performance	Confined E-field region	Disturbance analysis effect	High stability performance
				Max. FDR (GHz)	Max NS. (%)	Max Acc. (GHz)					
[8]	SRR	0.39	1 – 7.33	0.102	1.625	98.20	1	-	Yes	-	-
[10]	SSRR with spurlines	2.22	1 – 4.40	0.030	1.340	98.36	2	-	Yes	-	-
[13]	CSRR	2.65	1 – 3.00	0.150	5.380	97.71	2	-	Yes	-	-
[19]	IDC	2.65	1 – 6.15	0.373	4.300	99.99	2	-	Yes	-	-
[20]	IDC	2.35 / 5.79	1 – 10.5	0.150	3.980	99.99	2	-	Yes	-	-
[21]	Artificial Magnetic Conductor	4.04	1 – 4.40	0.070	1.890	96.48	1	-	Yes	-	-
[23]	Slot-loaded patch	2.50	1 – 10.20	0.072	5.240	98.80	1	-	-	-	-
[24]	Dual U-shaped	1.20 / 2.10	1 – 4.30	0.007	1.150	99.02	1	Yes	Yes	-	-
[25]	Aperture coupling	9.54 / 12.30	1 – 12.50	0.078	0.640	92.30	1	Yes	Yes	-	-
[26]	Dual T-shaped with IDC	1.64 / 2.43	1 – 6.15	0.016	0.003	95.99	1	Yes	Yes	-	-
[32]	SRR	1.24 / 2.08	1 – 6.00	0.050	4.101	96.97	2	Yes	Yes	-	-
This work	**Asymmetric branch feed with IDC**	**1.61 / 2.52**	**1 – 6.15**	**0.110**	**4.330**	**95.98**	**1`**	**Yes**	**Yes**	**Yes**	**Yes**

V. CONCLUSION

This paper has successfully designed and realized a high stability single port dual-band microwave sensor using interdigital structure with asymmetry branch feedline for solid material characterization with permittivity range 1 - 6.15. The proposed sensor operates at two different resonance frequencies f_{r1} = 1.61 GHz and f_{r2} = 2.52 GHz. Based on the measurement results, the proposed sensor has high stability both without and with disturbance for d = 1 cm – 2.5 cm with a Frequency Detection Resolution (FDR) of 0.009 - 0.4 GHz/$\Delta\varepsilon_r$, a Normalized Sensitivity (NS) of 0.4% - 4.4%, and an average accuracy of 90% - 95% for both resonance frequencies, respectively. Therefore, this sensor can be recommended for several applications including biomedical industry, medicine and material quality control especially for outdoor measurements that are potentially affected by electromagnetic interference and disturbance.

VI. ACKNOWLEDGMENT

This work is supported by Research and Community Services Institute of Universitas Trisakti and Ministry of Research, Technology and Higher Education of Republik Indonesia through a competitive research grant under the KATALIS Research Scheme fiscal year of 2024 with contract number of 058/E5/PG.02.00/PL.BATCH.2/2024 and 1091/LL3/AL.04/2024.

REFERENCES

[1] K. S. L. Parvathi and S. R. Gupta, "Ultrahigh-Sensitivity and Compact EBG-Based Microwave Sensor for Liquid Characterization," *IEEE Sensors Lett.*, vol. 6, no. 4, pp. 19–22, 2022, doi: 10.1109/LSENS.2022.3159800.

[2] A. Armghan, T. M. Alanazi, A. Altaf, and T. Haq, "Characterization of Dielectric Substrates Using Dual Band Microwave Sensor," *IEEE Access*, vol. 9, pp. 62779–62787, 2021, doi: 10.1109/ACCESS.2021.3075246.

[3] Z. Shaterian and M. Mrozowski, "Multifunctional Bandpass Filter/Displacement Sensor Component," *IEEE Access*, vol. 11, no. March, pp. 27012–27019, 2023, doi: 10.1109/ACCESS.2023.3258545.

[4] A. Aquino, C. G. Juan, B. Potelon, and C. Quendo, "Dielectric Permittivity Sensor Based on Planar Open-Loop Resonator," *IEEE Sensors Lett.*, vol. 5, no. 3, pp. 2021–2024, 2021, doi: 10.1109/LSENS.2021.3055544.

[5] W. A. Jabbar *et al.*, "Design and Fabrication of Smart Home with Internet of Things Enabled Automation System," *IEEE Access*, vol. 7, pp. 144059–144074, 2019, doi: 10.1109/ACCESS.2019.2942846.

[6] A. Ebrahimi, J. Scott, and K. Ghorbani, "Ultrahigh-Sensitivity Microwave Sensor for Microfluidic Complex Permittivity Measurement," *IEEE Trans. Microw. Theory Tech.*, vol. 67, no. 10, pp. 4269–4277, 2019, doi: 10.1109/TMTT.2019.2932737.

[7] P. Jahangiri, M. Naser-Moghadasi, B. Ghalamkari, and M. Dousti, "A new planar microwave sensor for fat-measuring of meat based on SRR and periodic EBG structures," *Sensors Actuators A Phys.*, vol. 346, no. June, p. 113826, 2022, doi: 10.1016/j.sna.2022.113826.

[8] K. Xu *et al.*, "Novel Microwave Sensors Based on Split Ring Resonators for Measuring Permittivity," *IEEE Access*, vol. 6, pp. 26111–26120, 2018, doi: 10.1109/ACCESS.2018.2834726.

[9] W. Liu, J. Zhang, and K. Huang, "Dual-Band Microwave Sensor Based on Planar Rectangular Cavity Loaded with Pairs of Improved Resonator for Differential Sensing Applications," *IEEE Trans.*

Instrum. Meas., vol. 70, 2021, doi: 10.1109/TIM.2021.3118090.

[10] R. A. Alahnomi, Z. Zakaria, E. Ruslan, S. R. Ab Rashid, and A. A. Mohd Bahar, "High-Q sensor based on symmetrical split ring resonator with spurlines for solids material detection," *IEEE Sens. J.*, vol. 17, no. 9, pp. 2766–2775, 2017, doi: 10.1109/JSEN.2017.2682266.

[11] M. Saadat-Safa, V. Nayyeri, M. Khanjarian, M. Soleimani, and O. M. Ramahi, "A CSRR-Based Sensor for Full Characterization of Magneto-Dielectric Materials," *IEEE Trans. Microw. Theory Tech.*, vol. 67, no. 2, pp. 806–814, 2019, doi: 10.1109/TMTT.2018.2882826.

[12] M. Abdolrazzaghi, N. Kazemi, V. Nayyeri, and F. Martin, "AI-Assisted Ultra-High-Sensitivity/Resolution Active-Coupled CSRR-Based Sensor with Embedded Selectivity," *Sensors*, vol. 23, no. 13, pp. 1–20, 2023, doi: 10.3390/s23136236.

[13] M. A. H. Ansari, A. K. Jha, and M. J. Akhtar, "Design and Application of the CSRR-Based Planar Sensor for Noninvasive Measurement of Complex Permittivity," *IEEE Sens. J.*, vol. 15, no. 12, pp. 7181–7189, 2015, doi: 10.1109/JSEN.2015.2469683.

[14] A. A. Mohd Bahar, Z. Zakaria, M. K. Md Arshad, R. A. Alahnomi, A. I. Abu-Khadrah, and W. Y. Sam, "Microfluidic biochemical sensor based on circular SIW-DMS approach for dielectric characterization application," *Int. J. RF Microw. Comput. Eng.*, vol. 29, no. 9, pp. 1–13, 2019, doi: 10.1002/mmce.21801.

[15] A. A. Mohd Bahar, Z. Zakaria, M. K. Md. Arshad, A. A. M. Isa, Y. Dasril, and R. A. Alahnomi, "Real Time Microwave Biochemical Sensor Based on Circular SIW Approach for Aqueous Dielectric Detection," *Sci. Rep.*, vol. 9, no. 1, pp. 1–12, 2019, doi: 10.1038/s41598-019-41702-3.

[16] J. Yeo and J. I. Lee, "High-sensitivity microwave sensor based on an interdigital-capacitor-shaped defected ground structure for permittivity characterization," *Sensors (Switzerland)*, vol. 19, no. 3, 2019, doi: 10.3390/s19030498.

[17] S. Aiswarya, S. K. Menon, M. Donelli, and L. Meenu, "Development of a microwave sensor for solid and liquid substances based on closed loop resonator," *Sensors*, vol. 21, no. 24, pp. 1–34, 2021, doi: 10.3390/s21248506.

[18] L. Ali *et al.*, "Design and optimization of microwave sensor for the non-contact measurement of pure dielectric materials," *Electron.*, vol. 10, no. 24, 2021, doi: 10.3390/electronics10243057.

[19] L. Ali *et al.*, "Design and Optimization of Interdigitated Microwave Sensor for Multidimensional Sensitive Characterization of Solid Materials," *IEEE Sens. J.*, vol. 21, no. 20, pp. 22814–22822, 2021, doi: 10.1109/JSEN.2021.3105410.

[20] C. Wang *et al.*, "High-Accuracy Complex Permittivity Characterization of Solid Materials Using Parallel Interdigital Capacitor-Based Planar Microwave Sensor," *IEEE Sens. J.*, vol. 21, no. 5, pp. 6083–6093, 2021, doi: 10.1109/JSEN.2020.3041014.

[21] W. J. Wu and G. Wang, "A modified AMC-based antenna sensor for contactless measurement of complex permittivity," *Meas. J. Int. Meas. Confed.*, vol. 206, no. June 2022, p. 112261, 2023, doi: 10.1016/j.measurement.2022.112261.

[22] Q. Shi, X. W. Xuan, H. K. Nie, Z. Y. Wang, and W. Wang, "Antenna Sensor Based on AMC Array for Contactless Detection of Water and Ethanol in Oil," *IEEE Sens. J.*, vol. 21, no. 19, pp. 21503–21510, 2021, doi: 10.1109/JSEN.2021.3102294.

[23] J. Yeo and J. I. Lee, "Slot-loaded microstrip patch sensor antenna for high-sensitivity permittivity characterization," *Electron.*, vol. 8, no. 5, 2019, doi: 10.3390/electronics8050502.

[24] S. Alam, Z. Zakaria, I. Surjati, N. A. Shairi, M. Alaydrus, and T. Firmansyah, "Dual-Band Independent Permittivity Sensor Using Single-Port with a Pair of U-Shaped Structures for Solid Material Detection," *IEEE Sens. J.*, vol. 22, no. 16, pp. 16111–16119, 2022, doi: 10.1109/JSEN.2022.3191345.

[25] M. Behdani, M. M. H. Kalateh, H. Saghlatoon, J. Melzer, and R. Mirzavand, "High-Resolution Dielectric Constant Measurement Using a Sensor Antenna with an Allocated Link for Data Transmission," *IEEE Sens. J.*, vol. 20, no. 24, pp. 14827–14835, 2020, doi: 10.1109/JSEN.2020.3012055.

[26] S. Alam *et al.*, "Collaboratively Far-Field and Near-Field Regions for Dual-Modalities Microwave Permittivity Sensor Using T-Shaped Resonator Embedded With IDC," *IEEE Sensors Lett.*, vol. 8, no. 7, pp. 8–11, 2024, doi: 10.1109/LSENS.2024.3415362.

[27] S. Alam, Z. Zakaria, I. Surjati, N. A. Shairi, M. Alaydrus, and T. Firmansyah, "Multifunctional of dual-band permittivity sensors with antenna using multicascode T-shaped resonators for simultaneous measurement of solid materials and data transfer capabilities," *Meas. J. Int. Meas. Confed.*, vol. 217, no. November 2022, p. 113078, 2023, doi: 10.1016/j.measurement.2023.113078.

[28] A. Ebrahimi, F. J. Tovar-Lopez, J. Scott, and K. Ghorbani, "Differential microwave sensor for characterization of glycerol–water solutions," *Sensors Actuators, B Chem.*, vol. 321, p. 128561, 2020, doi: 10.1016/j.snb.2020.128561.

[29] S. Kiani, P. Rezaei, and M. Navaei, "Dual-sensing and dual-frequency microwave SRR sensor for liquid samples permittivity detection," *Meas. J. Int. Meas. Confed.*, vol. 160, p. 107805, 2020, doi: 10.1016/j.measurement.2020.107805.

[30] S. Kiani, P. Rezaei, and M. Fakhr, "Real-Time Measurement of Liquid Permittivity Through Label-Free Meandered Microwave Sensor," *IETE J. Res.*, 2023, doi: 10.1080/03772063.2023.2231875.

[31] R. C. Caleffo and F. S. Correra, "Liquids electrical characterization sensor using a hybrid SIW resonant cavity," *Microw. Opt. Technol. Lett.*, vol. 60, no. 2, pp. 445–449, 2018, doi: 10.1002/mop.30983.

[32] A. A. Al-Behadili, I. A. Mocanu, N. Codreanu, and M. Pantazica, "Modified split ring resonators sensor for accurate complex permittivity measurements of solid dielectrics," *Sensors (Switzerland)*, vol. 20, no. 23, pp. 1–18, 2020, doi: 10.3390/s20236855.

[33] S. Lim, C. Y. Kim, and S. Hong, "Simultaneous Measurement of Thickness and Permittivity by Means of the Resonant Frequency Fitting of a Microstrip Line Ring Resonator," *IEEE Microw. Wirel. Components Lett.*, vol. 28, no. 6, pp. 539–541, 2018, doi: 10.1109/LMWC.2018.2833202.

Syah Alam was born in Jakarta, Indonesia. He received Bachelor Education of Engineering (S.Pd) degree in electrical engineering from Universitas Pendidikan Indonesia (UPI) and M.Eng (M.T) degree in telecommunication engineering from Graduate Programe of Electrical Engineering Universitas Trisakti in 2010 and 2012, respectively. In 2018, he joined the Department of Electrical Engineering Universitas Trisakti as a researcher and lecturer. In 2024, he is completed his PhD at Universiti Teknikal Melaka Malaysia (UTeM) in the field of Electronic Engineering (RF and Microwave). His research interests include microstrip antenna, and microwave sensors for various applications.

Indra Surjati was born in Bangkok, Thailand. She received Bachelor of Engineering (Ir.) degree in electrical engineering and M.Eng (M.T) degree in telecommunication engineering from Graduate Programe of Electrical Engineering Universitas Trisakti in 1996, respectively. In 2004 she completed his PhD in Electrical Engineering Department at the University of Indonesia and in 2011 she was confirmed as Professor in the Department of Electrical Engineering at Trisakti. Her research interests include microstrip antenna and microwave circuit for various applications.

Lydia Sari received the B.S. degrees in electrical engineering from Universitas Trisakti, Jakarta, Indonesia in 1998. She received the M.S. and Ph.D degrees in electrical engineering from University of Indonesia in 2002 and 2010, respectively. She is currently a faculty member in Electrical Engineering Department, Universitas Trisakti. Her research interests include wireless communications and information theory.

Raden Deiny Mardian received a bachelor's degree in 1998 and a master's degree in 2001, both in electrical engineering, from Universitas Trisakti, Jakarta, Indonesia. In early 2023 he received a doctoral degree in electrical engineering from Universitas Indonesia, Depok, Indonesia. He has published several journal papers and conference proceedings. He is currently a lecturer at the Electrical Engineering Department, Faculty of Industrial Technology, Universitas Trisakti, Jakarta, Indonesia. His research interests are mobile and wireless communication technology, digital broadcasting, quality of service, and quality of experience—all his research concerns technical and regulatory policy management.

Teguh Firmansyah, was born in Subang, Indonesia. He received a B.Eng. and M. Eng degree in electrical engineering from the Department of Electrical Engineering, Universitas Indonesia, in 2010 and 2012, respectively. In 2022, He received his Dr. Eng degree from Shizuoka University Japan as the best graduate. In 2012, he joined the Department of Electrical Engineering, Universitas Sultan Ageng Tirtayasa, as a Researcher and a Lecturer. He holds two patents for wideband antenna and multiband antenna. His research interests include microwave circuits for various applications and developing multifunctional sensors using acoustic, plasmonic, and microwave resonators.

Mudrik Alaydrus was born in Jakarta, Indonesia. He received the Dipl.-Ing. and Dr.-Ing. degrees in Electrical Engineering from Universitaet Hannover and Universitaet Wuppertal, in 1997 and 2001, respectively. Since 2003, he has worked at Universitas Mercu Buana, Jakarta. Dr. Alaydrus is Senior Member of IEEE and member of Verein der Deutschen Elektroingenieure (VDE). His current researchs include microwave and millimeter wave components, wireless power transfers, wireless sensor networks, interaction between electromagnetics and materials, and mathematical modeling in signal processing.

. **Zahrialdha Zakaria** was born in Johor, Malaysia. He received the B. Eng. and M. Eng. In Electrical and Electronic Engineering from the Universiti Teknologi Malaysia in 1998 and 2004 respectively, and the PhD degree in Electrical & Electronic Engineering from the Institute of Microwaves and Photonics (IMP), University of Leeds, United Kingdom in 2010. From 1998 to 2002, he was with STMicroelectronics, Malaysia where he worked as Product Engineer. He is currently a Professor at Microwave Research Group (MRG), Faculty of Electronic & Computer Engineering, University Teknikal Malaysia Melaka (UTeM). His research interests include variety of microwave devices development such as planar and nonplanar microwave filters, resonators, amplifiers and antennas. He also investigates energy harvesting and sensors.